FEBS Letters 587 (2013) 2912–2917

journal homepage: www.FEBSLetters.org

Structural peculiarities of the $(MHF1–MHF2)_4$ octamer provide a long DNA binding patch to anchor the MHF–FANCM complex to chromatin: A solution SAXS study

Wenjia Wang [a], Qiong Guo [b,c], Eleonora V. Shtykova [d], Guangfeng Liu [a], Jianhua Xu [a], Maikun Teng [b,c], Peng Liu [a,*], Yuhui Dong [a,*]

[a] Beijing Synchrotron Radiation Facility, Institute of High Energy Physics, Chinese Academy of Sciences, Beijing 100049, China
[b] Hefei National Laboratory for Physical Sciences at Microscale and School of Life Sciences, University of Science and Technology of China, Hefei, Anhui 230026, China
[c] Key Laboratory of Structural Biology, Chinese Academy of Sciences, Hefei, Anhui 230026, China
[d] Institute of Crystallography, Russian Academy of Sciences, 59 Leninsky Pr., Moscow 117333, Russia

ARTICLE INFO

Article history:
Received 15 April 2013
Revised 8 June 2013
Accepted 2 July 2013
Available online 22 July 2013

Edited by Gianni Cesareni

Keywords:
Fanconi anaemia
MHF complex
FANCM
DNA binding patch
SAXS

ABSTRACT

MHF1 and MHF2 are histone-fold-containing FANCM-associated proteins. FANCM is a Fanconi anemia (FA) complementation group protein. We previously obtained high-resolution structures of MHF1–MHF2 (MHF) and MHF in complex with a fragment of FANCM (MHF–FANCM-F). Here, we use small angle X-ray scattering (SAXS) to investigate the solution behaviors of these protein complexes. In combination with crystallographic data, the results of the SAXS study reveal that a long, positively charged patch exposed on the surface of the MHF complex plays a critical role in double-stranded DNA (dsDNA) binding.

Structured summary of protein interactions:
MHF2, **MHF1** and **FANCM-F** physically interact by molecular sieving (View interaction)
MHF1 and **MHF2** bind by X ray scattering (View interaction)
MHF1 and **MHF2** bind by molecular sieving (View interaction)
MHF1, **FANCM-F** and **MHF2** physically interact by X ray scattering (View interaction)

1. Introduction

Fanconi anemia (FA) is a rare multigenetic syndrome characterized by developmental defects, bone marrow failure and cancer predisposition [1–3]. Any defect in the 15 known *FANC* genes will induce failure of DNA damage repair, leading to FA [2–7]. FA cells are highly sensitive to agents that can cause DNA interstrand crosslinks (ICLs), which are abnormal structures blocking DNA replication. To combat ICLs, the FA core complex, composed of eight FA core proteins (FANCA, -B, -C, -E, -F, -G, -L and -M), is assembled at the damaged site recruiting additional FA factors to activate the FA pathway [3,8].

Being a component of the FA core complex, FANCM contains an evolutionarily conserved helicase domain and can specifically recognize and bind branched DNA structures [9–11]. Two histone-fold-containing proteins, MHF1 and MHF2, which show high affinity for double strand DNA (dsDNA), are FANCM-associated factors [12,13], and FANCM is targeted to the chromatin by binding to a compact $(MHF1–MHF2)_2$ tetramer [14].

The C-terminus of MHF1 plays a crucial role in DNA binding to both MHF and MHF–FANCM complexes [12,14], but its high-resolution structure is unknown, since the C region of MHF1 cannot be crystallized, possibly because of its flexibility. In the present work, to examine the full-length structures of MHF and of MHF in complex with a fragment of FANCM (MHF–FANCM-F) complexes in solution, small angle X-ray scattering (SAXS) was employed. The method analyzes a structure of an object at resolutions between 1 and 100 nm [15], thereby providing valuable structural information both about nano scale inhomogeneities (particles or clusters) and about the internal ordering in the sample. Advanced SAXS data processing and interpretation techniques, including ab initio and rigid body modeling methods [16,17] were used to reveal

Abbreviations: FA, Fanconi anemia; ICLs, interstrand crosslinks; dsDNA, double strand DNA; MHF, MHF1–MHF2; MHF–FANCM-F, MHF in complex with a fragment of FANCM; SEC, size-exclusion chromatography; MM, molecular mass

* Corresponding authors. Address: Institute of High Energy Physics, Chinese Academy of Sciences, 19B YuquanLu, Shijingshan District, Beijing 100049, China. Fax: +86 10 88233201.

E-mail addresses: liup@ihep.ac.cn (P. Liu), dongyh@ihep.ac.cn (Y. Dong).

0014-5793/$36.00 © 2013 Published by Elsevier B.V. on behalf of the Federation of European Biochemical Societies.
http://dx.doi.org/10.1016/j.febslet.2013.07.022

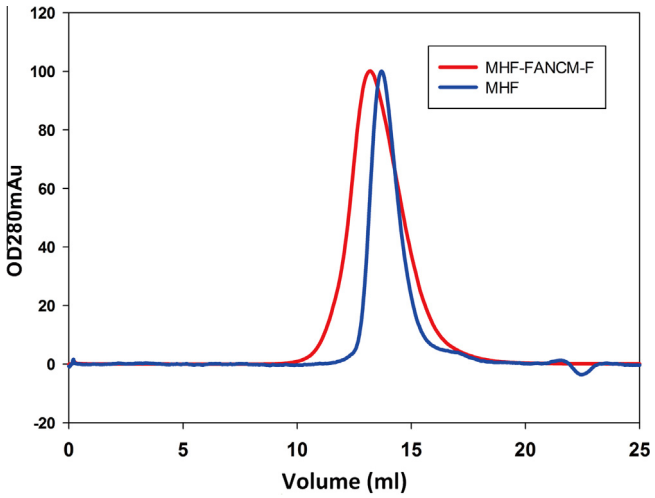

Fig. 1. Size-exclusion chromatography analysis of MHF and MHF–FANCM-F. Blue curve and red curve represent the SEC results of MHF and MHF–FANCM-F, respectively.

structural peculiarities of the MHF and MHF–FANCM-F complexes and to evaluate their roles in DNA damage repair and genome maintenance processes.

2. Materials and methods

2.1. Sample preparation

MHF and MHF–FANCM-F were expressed and purified as described previously [14]. The protein was passed through a Superdex 200 with the buffer 200 mM NaCl and 20 mM Tris–HCl, pH 7.5, as the last step of purification. The size-exclusion chromatography (SEC) results were also used for analyzing the molecular masses (MMs) of MHF and MHF–FANCM-F in solution.

2.2. Data collection

Two mM DTT was added into the sample just prior to SAXS data collection to avoid radiation damage. SAXS data were collected on the storage ring DORIS III of the Deutsches Elektronen Synchrotron (DESY, Hamburg, Germany) on the X33 beamline at the European Molecular Biology Laboratory (EMBL). Equipped with an automatic sample changer, all measurements were taken in vacuum to obtain a better signal-to-noise ratio. The scattering signal was recorded by a PILATUS detector (Dectris, Baden, Switzerland) in the range of the momentum transfer $0.02 < s < 0.55$ Å^{-1}, where $s = (4\pi\sin\theta)/\lambda$, 2θ is the scattering angle, and $\lambda = 1.5$ Å is the X-ray wavelength. Because of the high experimental noise for s values >0.22 Å^{-1}, the most informative part of the scattering data from 0.02 to 0.22 Å^{-1} was used for structural analysis. The measurements were carried out with exposure times of eight successive 15-s frames to monitor possible radiation damage (no radiation effects were detected). To account the interparticle interaction effects, solutions at protein concentrations of 4.0, 2.0 and 1.0 mg/ml were measured.

2.3. SAXS data processing

The SAXS data were processed using the ATSAS program package [18]. The experimental scattering profiles were corrected by the background scattering from the solvent, and processed using the program PRIMUS [19]. The corrected curves were then further extrapolated to infinitive dilution using standard procedures. Molecular masses of MHF and MHF–FANCM-F complexes in solution were evaluated from the extrapolated scattering intensities at zero angle $I(0)$. Radii of gyration of the two complexes were analyzed in the range of the Guinier approximation region $sRg \leqslant 1.3$, according to the equation:

$$I_{\exp}(s) = I(0)\exp(-s^2R_g^2/3) \quad (1)$$

The program CRYSOL [20] was used to evaluate theoretical scattering from the available high-resolution structures of MHF and MHF–FANCM-F complexes. The distance distribution functions $p(r)$ were obtained with the program GNOM [21] using an indirect inverse Fourier transformation:

$$p(r) = \frac{1}{2\pi^2}\int_0^\infty srI(s)\sin(sr)ds \quad (2)$$

Low-resolution shapes were reconstructed by two complementary ab initio methods, DAMMIN [16], employing a dummy atom (bead) model of a particle, and GASBOR [17], which employs a chain-like ensemble of dummy residues. Starting from a random assembly, DAMMIN and GASBOR used simulated annealing protocols to build models fitting the experimental data $I_{exp}(s)$ to minimize a discrepancy. Ten models obtained from different program runs were compared and averaged using the program DAMAVER [22].

In addition, given the available high-resolution structures of $(MHF1–MHF2)_2$ and $(MHF1–MHF2)_2$–FANCM-F as subunits of the complexes, the program SASREF [23] was used to determine the relative positions of the subunits. The resultant SASREF models were superimposed with the averaged ab initio models using the program SUPCOMB. The program represents each input structure as an ensemble of points and minimizes a normalized spatial discrepancy (NSD) to find the best alignment of the two models. NSD is a measure of quantitative similarity between sets of three-dimensional points [24]. Binding affinities between two molecules of $(MHF1–MHF2)_2$ tetramers were calculated with PISA online [25].

The program CORAL [23] was used to reconstruct missing fragments of the available crystal structures using the full amino acid sequences and the available high-resolution structures. Electrostatic surfaces of the models were obtained and analyzed by the program PYMOL [26].

3. Results

3.1. Solution statuses of MHF and MHF–FANCM-F

In the present work, the solution structures of two complexes were studied: MHF (containing full-length MHF1 and MHF2) and MHF–FANCM-F (containing full-length MHF and a fragment of FANCM, residues 661–800). SEC results demonstrated that both MHF and MHF–FANCM-F do not aggregate and are well behaved single species with exclusion volumes of 13.7 and 13.2 ml, respectively (Fig. 1), corresponding to molecular masses (MMs) of ~100 kDa for MHF and ~115 kDa for MHF–FANCM-F. Theoretical MMs calculated for $(MHF1–MHF2)_2$ and $(MHF1–MHF2)_2$–FANCM-F are 49 and 66 kDa, respectively. These theoretical MMs are one half of those obtained by SEC, indicating the complexes form oligomeric species in solution.

SAXS profiles for MHF and MHF–FANCM-F are shown in Fig. 2. Previously obtained high-resolution structures of the samples are presented in Fig. 3A and B. Using these high-resolution structures the theoretical scattering curves computed by CRYSOL yield poor fits to the experimental SAXS data (Fig. 2, A and B, curves 2), pointing to a significant difference in overall shape between the crystal and solution states. The calculated distance distribution functions

for MHF and MHF–FANCM-F in the crystal and solution forms (Fig. 2A and B, inserts) also differ considerably. The corresponding structural parameters of the two complexes are listed in Table 1. Molecular masses evaluated from SAXS data are approximately two times more than the MMs for $(MHF1–MHF2)_2$ and $(MHF1–MHF2)_2$–FANCM-F, therefore agreeing with the SEC results. The radii of gyration and maximum diameters in solution are also greater than those calculated using the high-resolution structures. Hence, we postulate that MHF and MHF–FANCM-F in solution exist as $[(MHF1–MHF2)_2]_2$ and $[(MHF1–MHF2)_2–FANCM-F]_2$.

3.2. Ab initio shape reconstruction

Profiles of distance distribution functions for MHF and MHF–FANCM-F in solution (Fig. 2, inserts, curves 1) are characteristic for elongated bodies with cross-sections of about 40 Å and maximal sizes of ~125 Å. The functions were further used for low-resolution shape restorations.

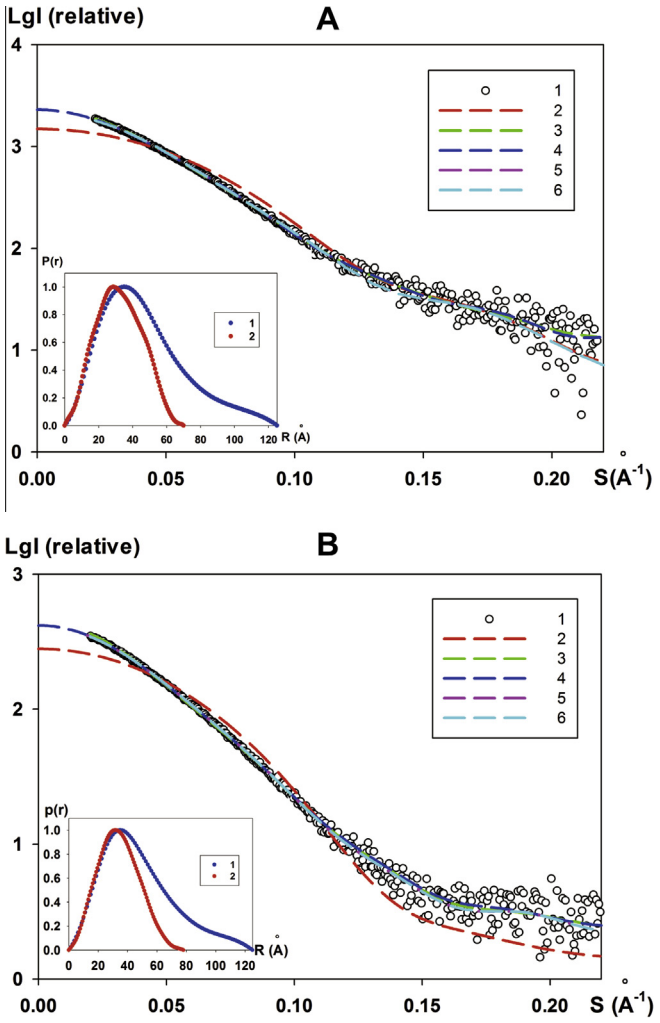

Fig. 2. SAXS patterns and modeling. (A) SAXS scattering data from MHF in solution: 1 – experimental data; 2 – scattering pattern computed from the crystal structure; 3 – scattering pattern computed from the ab initio model; 4 – smooth curve back transformed from the $p(r)$ and extrapolated to zero scattering angle for MHF; 5 – scattering pattern computed from the SASREF model; 6 – scattering pattern computed from the CORAL model. Insert: left below – the distance distribution function $p(r)$ computed by the program GNOM for MHF in solution (curve 1) and the theoretical $p(r)$ function calculated from the crystal structure of MHF (curve 2). (B) SAXS scattering data of MHF–FANCM-F in solution: Curves 1–6 and the insert represent the same derived profiles for MHF–FANCM-F as defined in (A).

Ab initio shape reconstructions performed using programs DAMMIN and GASBOR yielded reproducible results fitting experimental data with discrepancies of 1.17 and of 1.28 for MHF and MHF–FANCM-F, respectively (Fig. 2A and B, curves 3). The corresponding smooth curve back transformed from the $p(r)$ functions and extrapolated to zero scattering angle also demonstrated good approximations of the experimental profiles (Fig. 2A and B, curves 4). Fig. 4A (left column) shows the model of MHF obtained by the ab initio procedure is a 'double-V' shape, which can be considered as two $(MHF1–MHF2)_2$ molecules, arranged one by one and slightly rotated relative to each other. The ab initio model of MHF–FANCM-F has a pillar-like shape and also can be described as two $(MHF1–MHF2)_2$–FANCM-F subunits arranged one after another (Fig. 4B, left column).

3.3. Rigid body modeling

To determine a spatial organization of the specimens, we searched throughout their crystals for possible interactions. For MHF, one asymmetric unit consists of two molecules of $(MHF1–MHF2)_2$. Three possible formations of $[(MHF1–MHF2)_2]_2$ (Fig. S1) were selected and checked against the SAXS data, resulting in bad approximations to the SAXS profiles. In addition, the binding affinities at the interfaces between two molecules of $(MHF1–MHF2)_2$ were very low according to PISA analysis (the solvation free energy for each model is shown in *Fig.* S1). As for MHF–FANCM-F, there are three molecules of $(MHF1–MHF2)_2$–FANCM-F in one asymmetric unit, which is obviously different from the solution formation.

According to the analysis above, we propose that the process of crystallization destroyed the interactions between two subunits due to packing forces. As a result, a new model should be built based on the SAXS data. The program SASREF and the method molecular tectonics were applied using the available atomic structures of $(MHF1–MHF2)_2$ and $(MHF1–MHF2)_2$–FANCM-F as subunits for rigid body modeling. The results of the reconstructions are presented in Fig. 4, second column. The obtained models yield good fits to the experimental SAXS data with discrepancies of 1.07 and 1.13 for MHF and MHF–FANCM-F, respectively (Fig. 2A and B, curves 5). Moreover, the interaction between two molecules of $(MHF1–MHF2)_2$ in the SASREF model is much greater than observed in the crystal form (Fig. S1), indicating a more reasonable model for the octamer. Importantly, the SASREF reconstructions are in good agreement with the ab initio models as demonstrated by the program SUPCOMB (Fig. 4, third column, NSD = 1.37 for MHF and NSD = 1.51 for MHF–FANCM-F). Thus, two independent methods gave consistent results, thereby supporting the notion that the models presented here clearly represent solution structures.

3.4. Restoration of missing fragments

Given the amino acid sequences of MHF1, MHF2 and FANCM-F, the C-terminus of MHF1 (residues 108–138) were further restored by the program CORAL. The results of the restorations are shown in Fig. 4 (right column). Restorations of the missing C-ends of MHF1 for MHF and MHF–FANCM-F complexes were performed using SASREF models as a basis. The octameric structure of MHF was divided into separated MHF1–MHF2 units, and the four missing C-termini were embedded by the program CORAL into each MHF1–MHF2 unit. Several different formations of loops (Fig. S2) were generated with different discrepancies to the experimental data, from which the one fitting best was chosen as the final model. Similarly, for MHF–FANCM-F, the SASREF model was divided into six parts, four MHF1–MHF2 hetero-dimers and two FANCM-F fragments, and then the C-terminal domains of MHF1 were restored. In both

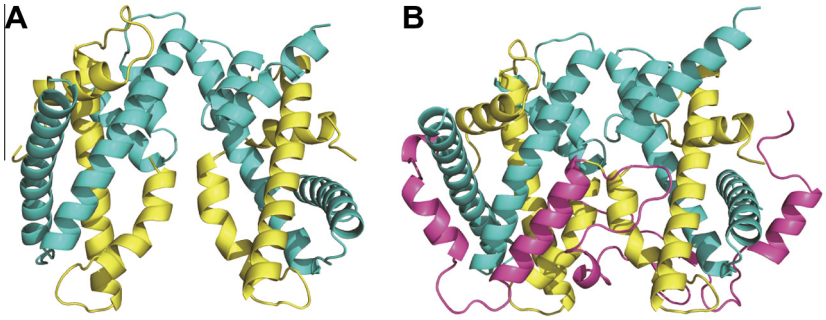

Fig. 3. Crystal structures of MHF and MHF–FANCM-F. (PDB id: 4DRA, 4DRB) (A) MHF acts as a hetero-tetramer in the crystal with two MHF1 (residues 1–114, colored in blue) and two MHF2 (full length, colored in yellow) proteins combine tightly with each other. (B) A fragment of FANCM (residues 661–800, colored in magenta) binds tightly to the $(MHF1–MHF2)_2$ tetramer to form a 'double-V' shape appearance. (For interpretation of the references to colour in this figure legend, the reader is referred to the web version of this article.)

Table 1
The overall parameters of MHF and MHF–FANCM calculated from the SAXS data (SAXS) and from the theoretical crystallography values (crystal), including the radius of gyration (R_g), molecular mass (MM) and maximum diameter (D_{max}).

Sample	R_g (nm)		MM (kDa)		D_{max} (nm)	
	SAXS	Crystal	SAXS	Crystal	SAXS	Crystal
MHF	3.42 ± 0.03	2.15	92 ± 3	49	125 ± 3	70
MHF–FANCM	3.67 ± 0.02	2.28	125 ± 2	66	126 ± 3	79

cases, good fits to the experimental scattering curves were obtained with discrepancy of 1.03 for MHF and 0.91 for MHF–FANCM-F (Fig. 2A and B, curves 6). The results of the restorations by the program CORAL demonstrate that the C-terminus of the MHF1 protein is flexible, weakly ordered and protrudes slightly from the main structure into the bulk solution.

The electronic surfaces of MHF and MHF–FANCM-F obtained from the SASREF models are presented in Fig. 5. Positively charged

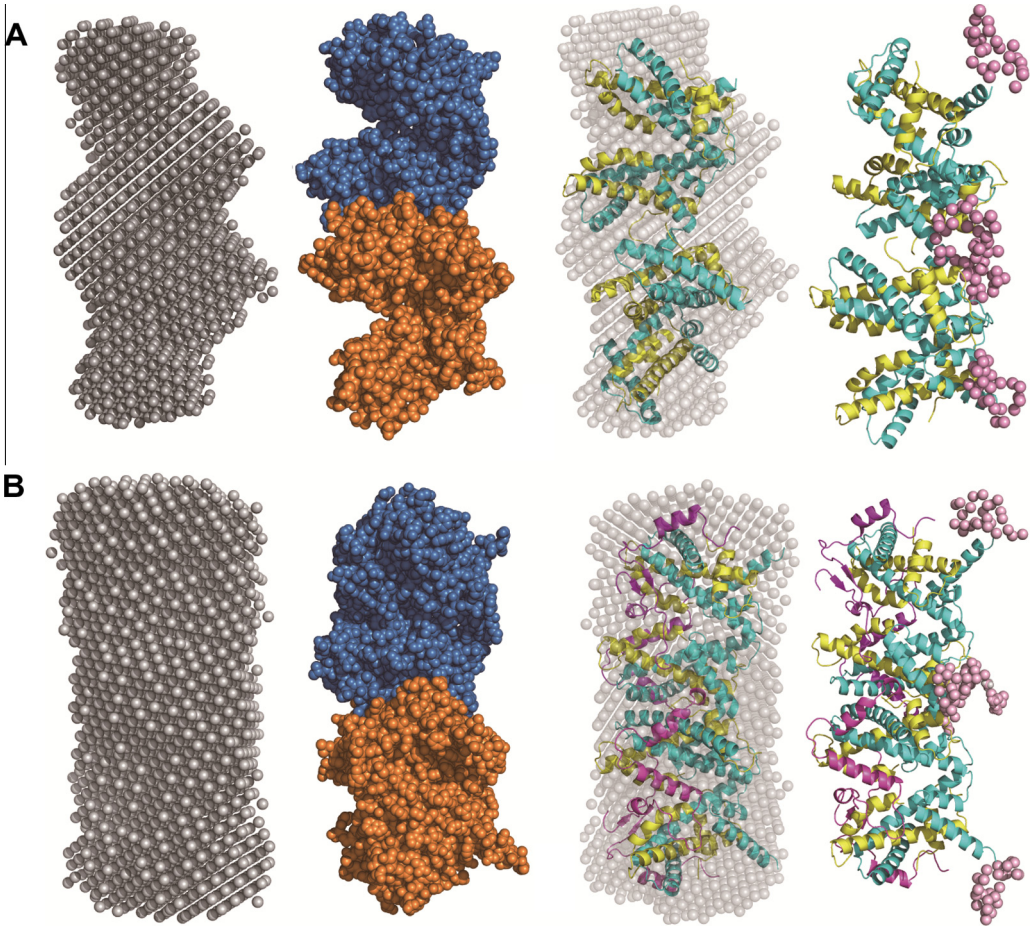

Fig. 4. Models generated by SAXS. (A) SAXS models for the MHF complex in solution. (B) SAXS models for MHF–FANCM-F in solution. First column: averaged ab initio models from DAMMIN and GASBOR models. Second column: typical models calculated from SASREF. Third column: superposition of ab initio models and rigid body models by the program SUPCOMB. Last column: final models with the missing loops of MHF1 generated by the program CORAL. The colors of the high-resolution structures are the same as used in Fig. 2, and the missing loops are represented as dummy residues colored pink. (For interpretation of the references to colour in this figure legend, the reader is referred to the web version of this article.)

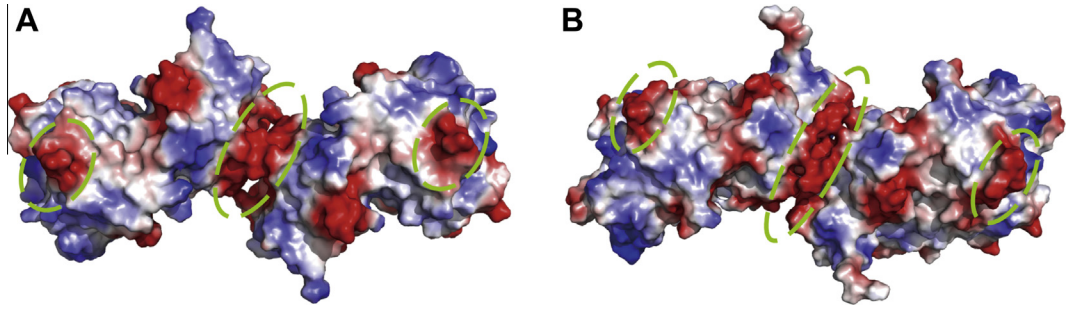

Fig. 5. Electrostatic surface analysis of MHF and MHF–FANCM-F on the convex side. (A) and (B) represent the electrostatic surface diagrams for MHF and MHF–FANCM-F separately (blue represents a positively charged surface region and red represents a negatively charged surface region). The green circles signify where the C-terminus of MHF1 should be located.

patches of MHF and MHF–FANCM are located at the junction of two parts of the complexes. Moreover, the CORAL models demonstrate that the negatively charged areas are concealed by the C-terminal ends of MHF1.

4. Discussion

FANCM, the only subunit of the FA core complex that binds DNA, acts mainly as an anchor required for the recruitment of the FA core complex to chromatin. [9–11] MHF1 and MHF2 are recently discovered partners of FANCM, and function to assist FANCM target chromatin, and can promote FANCM in the Holliday junction migration process [12,13].

In this investigation, SAXS was applied to determine the solution structures of the intact MHF and MHF–FANCM-F. Ab initio analysis and rigid body modeling were used independently and gave consistent results, showing a reliable construction and spatial organization of the two complexes. The SAXS-derived models are assemblies of $[(MHF1–MHF2)_2]_2$ and $[(MHF1–MHF2)_2–FANCM-F]_2$ in solution, and both complexes show elongated shapes that can be considered as two $(MHF1–MHF2)_2$ or $(MHF1–MHF2)_2$–FANCM-F subunits stacked on each other. It should be stressed that the conformations of the two complexes in solution were obtained independently for MHF and MHF–FANCM-F. Therefore, the similar architectures of the two complexes indicate that binding of the fragment of FANCM does not affect the overall architecture of MHF at this resolution. Moreover, the $(MHF1–MHF2)_2$ tetramer retains a rigid structure upon binding with FANCM-F according to crystallography analysis [14]. Based on these observations, we deduce that the intact MHF1 forms a hetero-octamer with MHF2 in solution, and each tetramer acts as a rigid scaffold to bind one molecule of FANCM.

The C-terminus of MHF1, which plays a critical role in DNA binding activity, was restored successfully into the solution SAXS models and was found to protrude slightly from the main structure and into the bulk solvent. The flexibility of the C-terminal region explains the difficulty to crystallize this region, and this mobility may be responsible for the ability of the domain to mediate different interactions.

Although being a low-resolution method, SAXS can provide useful overall structural information that is highly relevant to its biological function. The elongated octameric structure of MHF described in the present work is consistent with its DNA binding activity. The electrostatic surfaces of both MHF and MHF–FANCM-F obtained from the SAXS models (Fig. 5) demonstrate that the higher oligomeric states generate large positively charged patches that were not observed in the crystal structures. Thus, the larger positive surface is likely to further stabilize the interaction between MHF and chromatin. Additionally, all C-terminal parts of MHF1 locate on the negative electrostatic sites of the convex side. This observation explains the indispensability of the C-terminal fragments of MHF1 for DNA binding. These fragments can cover the negatively charged regions, connect the two positively charged patches and can possibly act as binding handles for conjunction to dsDNA.

According to the SAXS models and to the structural analysis above, we propose that the elongated octameric architecture of MHF forms a good sliding groove for DNA binding and moving activity. It is known that MHF is essential for FANCM to form a stable association with chromatin, and that FANCM acts as an anchor required for the recruitment of the FA core complex [9–13]. Based on the two points above, we strongly suggest that the MHF octamer provides a 'landing pad' for the whole FA core complex (Fig. 6). Together with FANCM, MHF may translocate across replicating DNA along the sliding groove, thereby opening chromatin to allow the FA core complex to load. It is similar to the previous model [27], although there are obvious differences. First, for the first time MHF was added to the whole FA complex model and is hypothesized to be a 'landing pad' for the whole FA complex; rather than FANCM. Second, it is now clear that the basement of the FA core complex includes two molecules of FANCM, which indicates two FA core complexes working together to complete their functional assembly (Fig. 6).

Structural studies using crystallographic methods along with biochemical information about MHF and FANCM have provided

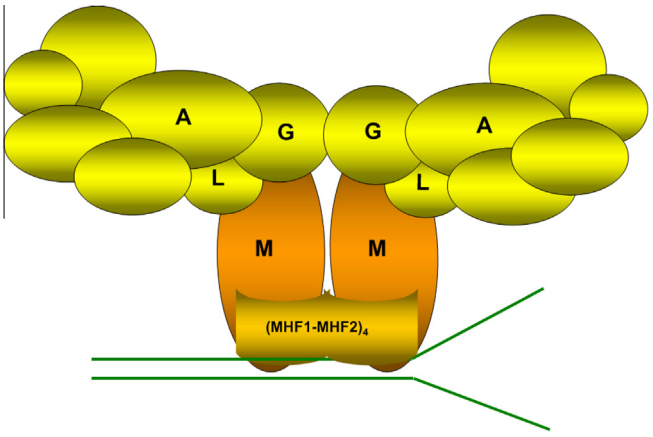

Fig. 6. Model for the role of MHF and FANCM in regulating the FA pathway in the S phase. The MHF complex combines two molecule of FANCM, whereas this MHF complex can also bind tightly to the stalled replication fork, thereby enhancing the association of FANCM to the chromatin significantly. In the S phase, phosphorylated FANCM can recruit the FA core complex to chromatin, possibly to replication forks, and together with MHF they provide a 'landing pad' for the whole FA complex.

information on the overall mechanism of the complex. However, the SAXS models are the first to elaborate the hetero-octameric structure of MHF, which is obviously different from its crystal structure. In particular, the location of C domains of MHF1 restored by SAXS is crucial for understanding the mechanism of MHF in DNA binding activity. Combining these models with our previously published high-resolution structures provide a better understanding of the mechanism in which the MHF–FANCM complex recruits the whole FA core complex and anchors it to the chromatin.

Acknowledgments

We are grateful to the staff members of DESY and SSRF for sample test and data collection. We also thank Dr. Yuyong Tao, Zengqiang Gao and Kun Qu for helpful discussion.

This work was supported by the Grants from the National Basic Research Program of China (2009CB918600) and National Natural Science Foundation of China (10979005).

Appendix A. Supplementary data

Supplementary data associated with this article can be found, in the online version, at http://dx.doi.org/10.1016/j.febslet.2013.07.022.

References

[1] D'Andrea, A.D. and Grompe, M. (2003) The Fanconi anaemia/BRCA pathway. Nat. Rev. Cancer 3, 23–34.
[2] de Winter, J.P. and Joenje, H. (2009) The genetic and molecular basis of Fanconi anemia. Mutat. Res. 668, 11–19.
[3] Wang, W. (2007) Emergence of a DNA-damage response network consisting of Fanconi anaemia and BRCA proteins. Nat. Rev. Genet. 8, 735–748.
[4] Kee, Y. and D'Andrea, A.D. (2010) Expanded roles of the Fanconi anemia pathway in preserving genomic stability. Genes Dev. 24, 1680–1694.
[5] Vaz, F. et al. (2010) Mutation of the RAD51C gene in a Fanconi anemia-like disorder. Nat. Genet. 42, 406–409.
[6] Kim, Y. et al. (2011) Mutations of the SLX4 gene in Fanconi anemia. Nat. Genet. 43, 142–146.
[7] Stoepker, C. et al. (2011) SLX4, a coordinator of structure-specific endonucleases, is mutated in a new Fanconi anemia subtype. Nat. Genet. 43, 138–141.
[8] Thompson, L.H. and Hinz, J.M. (2009) Cellular and molecular consequences of defective Fanconi anemia proteins in replication-coupled DNA repair: mechanistic insights. Mutat. Res. 668, 54–72.
[9] Meetei, A.R. et al. (2005) A human ortholog of archaeal DNA repair protein Hef is defective in Fanconi anemia complementation group M. Nat. Genet. 37, 958–963.
[10] Gari, K., Decaillet, C., Stasiak, A.Z., Stasiak, A. and Constantinou, A. (2008) The Fanconi anemia protein FANCM can promote branch migration of Holliday junctions and replication forks. Mol. Cell 29, 141–148.
[11] Gari, K., Decaillet, C., Delannoy, M., Wu, L. and Constantinou, A. (2008) Remodeling of DNA replication structures by the branch point translocase FANCM. Proc. Natl. Acad. Sci. 105, 16107–16112.
[12] Singh, T.R. et al. (2010) MHF1–MHF2, a histone-fold-containing protein complex, participates in the Fanconi anemia pathway via FANCM. Mol. Cell 37, 879–886.
[13] Yan, Z. et al. (2010) A histone-fold complex and FANCM form a conserved DNA-remodeling complex to maintain genome stability. Mol. Cell 37, 865–878.
[14] Tao, Yuyong. (2012) Et al. The structure of the FANCM–MHF complex reveals physical features for functional assembly. Nat. Commun. 3, 782.
[15] Mertens, H.D. and Svergun, D.I. (2010) Structural characterization of proteins and complexes using small-angle X-ray solution scattering. J. Struct. Biol. 172 (1), 128–141.
[16] Svergun, D.I. et al. (1999) Restoring low resolution structure of biological macromolecules from solution scattering using simulated annealing. Biophys. J. 76, 2879–2886.
[17] Petoukhov, M.V. and Svergun, D.I. (2005) Global rigid body modelling of macromolecular complexes against small-angle scattering data. Biophys. J. 89, 1237–1250.
[18] Konarev, P.V., Petoukhov, M.V., Volkov, V.V. and Svergun, D.I. (2006) ATSAS 2.1, a program package for small-angle scattering data analysis. J. Appl. Crystallogr. 39, 277–286.
[19] Konarev, P.V., Volkov, V.V., Sokolova, A.V., Koch, M.H.J. and Svergun, D.I. (2003) PRIMUS: a Windows PC-based system for small-angle scattering data analysis. J. Appl. Crystallogr. 36, 1277–1282.
[20] Svergun, D.I., Barberato, C. and Koch, M.H.J. (1995) CRYSOL – a program to evaluate X-ray solution scattering of biological macromolecules from atomic coordinates. J. Appl. Crystallogr. 28, 768–773.
[21] Svergun, D.I. et al. (1992) Determination of the regularization parameter in indirect-transform methods using perceptual criteria. J. Appl. Crystallogr. 25, 495–503.
[22] Volkov, V.V. and Svergun, D.I. (2003) Uniqueness of ab initio shape determination in small angle scattering. J. Appl. Crystallogr. 36, 860–864.
[23] Petoukhov, M.V. and Svergun, D.I. (2005) Global rigid body modelling of macromolecular complexes against small-angle scattering data. Biophys. J. 89, 1237–1250.
[24] Kozin, M.B. and Svergun, D.I. (2001) Automated matching of highand low-resolution structural models. J. Appl. Crystallogr. 34, 33–41.
[25] Krissinel, E. and Henrick, K. (2007) Inference of macromolecular assemblies from crystalline state. J. Mol. Biol. 372, 774–797.
[26] Delano, W.L. (2002) PyMOL Molecular Viewer. <http://www.pymol.org/>.
[27] Kim, J.M., Kee, Y., Gurtan, A. and D'Andrea, A.D. (2008) Cell cycle-dependent chromatin loading of the Fanconi anemia core complex by FANCM/FAAP24. Blood 111, 5215–5222.